Proceedings of the International Gas Turbine Congress 2003 Tokyo
November 2-7, 2003

IGTC2003Tokyo TS-048

Unsteady Three-Dimensional Navier-Stokes Simulations of Turbine Rotor-Stator Interaction Using Multi-Airfoil

Debasish Biswas, Tomonao Takamatsu and Hideo Iwasaki
Toshiba Corporation
Research and Development Center
Kawasaki, Japan

ABSTRACT

Understanding of complex unsteady flow behavior caused by the relative movement of the rotor with respect to stator is very important to improve current turbomachinery designs. However, in order to predict the measured temporal behavior accurately, it is necessary to consider the ratio of the rotors to stators equal to the actual case. Also, since the wake leaving the stators periodically impinging to the rotors, there occur considerable vortex stretching and change in turbulence activity in the rotor blade passages. In this study unsteady N-S equations using an improved turbulence model are solved for flow problem within axial turbine stage (the ratio of rotors to stators is equal to experimental value). The relative motion between the stator and rotor airfoils is made possible with the use of patched grids that move relative to each other. Assessment of computed results with the measured data showed a good agreement..

INTRODUCTION

In order to optimizing the performance of turbomachinery, it is very useful to have an accurate numerical analysis of the flows associated with stator-rotor configurations. However, flows within the turbomachinery are generally unsteady in nature and are therefore difficult to compute. The unsteadiness is caused by (a) the interaction of the rotor airfoils with the wakes and passage vortices generated by upstream airfoils, (b) the relative motion of the rotors with respect to the stators (potential effect), and (c) the shedding of vortices by the airfoils because of blunt trailing edges. Computation of such flow is further complicated by the relative motion between the rotor and stator airfoils and the periodic transition of flow from laminar to turbulent. However, in order to improve the current design procedures a clear understanding of the unsteady process within turbomachinery is very much necessary.

Over the past two decades steady progress has been made in the development of fluid flow analyses for turbomachinery blade rows. The eventual goal of these analyses is a time accurate model of the three-dimensional flow through the blade rows. In recent years, several papers on turbomachinery blade row computation are published. Several approach using two and three-dimensional Euler and Navier-Stokes equations for isolated blade rows and stator-rotor interaction are presented. Cascade flows are important to acquire a good understanding of the laminar to turbulent flow transition phenomena, interaction of shock and bondary layer, separation etc. However, information regarding the periodic transition of the flow resulted by the relative motion of the rotors with respect to the stator can not be obtained by such flow analyses. Dring et al.(1982) in his experimental work showed that the temporal pressure fluctuation near the leading edge of the rotor airfoil can be as much as 72 percent of the exit dynamic pressure, when the axial gap is reduced to 15 percent of the chord length (for the operating conditions and geometry chosen). Therefore, it is very much essential to consider the stator and rotor airfoils as a system in cases where interaction effects are predominant.

It is very difficult and even impractical to treat both the stator and rotor by a single computational domain. Since it would result in considerable distortion of the stator and rotor to provide the rotor motion. Consideration of zonal grid is the obvious solution to this problem. Typically, a set of stationary grids to treat the stator airfoils and a set of moving grids (stationary with respect to the rotor) to treat the rotor airfoils can be used. Then, based on special boundary conditions, information between the several grids can be transferred..

Rai(1987a),(1987b) presented two and three dimensional rotor stator interaction results for an axial turbine. The airfoil geometry and flow conditions used in their studies were same as those in the experiments of Dring et al. The unsteady thin layer N-S equations were solved in time accurate manner to obtain the unsteady flow field associated with this configuration. The governing equations were solved on a system of patched and overlaid grids with information transfer from grid to grid taking place at the zonal boundaries. The numerically obtained results are compared with the experimental results of Dring et al.(1982). In the two-dimensional case, a good comparison between theory and experiment is obtained in the case of time averaged pressures on the rotor and stator airfoils. Pressure amplitudes corresponding to the pressure variation in time were found to compare reasonably with the experiment in their study.

Later, in Rai (1987b) the approximation of two-dimensionality is removed and fully three-dimensional airfoils geometries are used. In addition, the hub, outer casing, and rotor tip clearance are all included in the calculations. As in Rai(1987a), a system of patched and overlaid grids is used to discretize the rather complex geometry of the three-dimensional configuration. An implicit, upwind third order accurate method is used in all the patches (the calculation of Rai(1987a) used hybrid upwind/central difference scheme near the surface boundaries). The equations solved are the unsteady, thin layer, Navier-Stokes equations in three dimensions. As in Rai(1987a), time-averaged airfoil surface pressure were found to compare well with experiment, but numerically obtained pressure amplitudes were only reasonably close to experimental data.

One approximation that was made by Rai (1987a), (1987b) was re-scaling of the rotor geometry. The experimental turbine of Dring et al.(1982) has 22 airfoils in the stator row and 28 airfoils in the rotor row. Therefore an accurate calculation would require a minimum of 25 airfoils (11 in stator row and 14 in rotor row). In order to avoid the computational expense involved in simulating the flow associated with 25 airfoils, the rotor airfoils was enlarged by a factor of 28/22, keeping the pitch to chord ratio the same. It was then assumed that there were 22 airfoils in the rotor row. This assumption makes it possible to perform a calculation with only one rotor and one stator, thus reducing computation time by more than one order of magnitude. Whereas, this approximation has little or no effect on time averaged pressure distributions, it does affect the temporal variation of the flow variables. Far-field acoustics are significantly altered when the configuration is changed to have an equal number of rotor and stator airfoils.

Later, Rai(1990) performed some computations using a solver that

Manuscript Received on July 7, 2003

could simulate flow in a stage with an unequal number of rotor and stator airfoils. The calculations were performed with the unsteady, thin layer Navier-Stokes equations in two-dimensions. The region of interest was discretized with the help of multiple patched and overlaid grids as in his previous work (1987a), (1987b). Results in the form of time-averaged pressures, as well as pressure amplitudes for the rotor and stator airfoils, were presented for both the one-stator/one-rotor and three-stator/four-rotor airfoil cases. Time averaged pressures were almost identical for the two cases. However, a significant improvement is obtained in pressure amplitude and phase for the three-stator/four rotor case. He mentioned that the improvement was expected to be due to the ratio of rotors to stators in the multi-airfoil calculation (4/3) is much closer to the experimental value (28/22). The degree of rotor re-scaling required to keep the blockage effects the same is much smaller.

Since the re-scaling approximation does affect the temporal variation of the flow variables. Far field acoustics are significantly altered when the configuration is changed to have an equal number of stator and rotor airfoils. To predict experimentally measured temporal behavior more accurately, in the present study, 11 stator and 14 rotor airfoils are considered. Patched grids are used to discretize the rather complex three-dimensional regions surrounding the rotor-stator configurations. In addition, the hub, outer casing and tip clearance are all included in computation model. No overlaid grids are used, because overlaid grid calculations are difficult to make conservative at the overlay boundaries. Also, an improved two-equation low-Reynolds number k-τ turbulence model developed by the author by including exact viscous term and by introducing wall damping functions with improved asymptotic behavior is used to predict the periodic transition of flow from laminar to turbulent. The model is proposed to reproduce the wall-limiting behavior of turbulence, the correct stream-wise blending between a pre-transitional pseudo-laminar boundary layer and post transitional fully turbulent boundary layer under the experimental effect of free-stream turbulence and pressure gradient. Also two major problems associated with k-ε model ((a) lack of natural boundary conditions for the dissipation rate and (b) the appearance of higher order correlation in the balance term of the dissipation rate at the wall.) are avoided by proposing a k-τ model. By including the exact viscous term and by introducing wall damping functions with improved asymptotic behavior, the present k-τ model (where, τ=k/ε, the turbulent time scale) is developed. It is demonstrated by Biswas(2002) that this model yields improved predictions for transitional boundary layer.

COMPUTATION MODEL

In the present section grid topology, and computation scheme, will be discussed.

Grid System for Stator-Rotor Configuration

Patched grids are used to discretize the regions surrounding the rotor-stator configuration. Since overlaid grid calculations are difficult to make conservative at the overlay boundaries. In the present study, the airfoil geometry used in the experimental investigation of Dring(1982) was used. The geometry comprises 28 rotor and 22 stator airfoils. In order to perform an accurate computation of temporal behavior in the flow passage, eleven stator airfoils and 14 rotor airfoils are used. Fig.1 shows the rotor-stator geometry of Dring(1982) at mid-span. The multi-zone grid used to discretize the region consists of 39 zones. 11 zonal grids for 11 stator configurations, 14 zonal grids for 14 rotor configurations and 14 zonal grids to cover the region of tip clearance. All the zones are discretized with H-grid. Fig.2(a) and (b) shows the grid for rotor and stator at the mid-span. Although the actual grids used for the calculations are very dense near the airfoil surfaces (to resolve the viscous effects), for the purpose of clarity fig.2 shows grids in which some points are omitted in the direction normal to the airfoil surfaces.

The outlet of 11 zonal grids for stator patched to the inlet of 14 zonal grids for rotor and slip past each other as the rotor airfoil moves downward. It is advantageous to use a patch boundary (as opposed to an area of overlay) where one system of grids moves relative to another system of grids because both time accuracy and conservation can be more easily controlled in patched grid calculations.

Numerical Methodology

In the present work, unsteady three-dimensional N-S equations are solved using an efficient IAF finite difference scheme of second order accuracy in time. In this approach, fully implicit finite difference equations are solved performing several iterations at each time step to make factorization and linearization errors zero. Also, to make the present approach robust, third order accurate TVD scheme based on MUSCL type approach with Roe's approximate Riemann solver is used. There are several boundaries that are used in the present calculation. These boundaries serve to separate the various zones. The zonal boundary conditions must meet certain requirements before they can be used effectively. The various zonal boundary calculations are made conservative for all the patch boundaries. Description of boundary condition at each of these boundaries is given in brief below.

At the wall boundaries, which correspond to airfoil surface, hub and end wall no-slip condition for velocity and adiabatic wall conditions for temperature is specified. In the case of rotor, which is moving relative to the stator, the relative velocity not the absolute velocity is set to zero at the wall. In the case of pressure, the derivative of pressure with respect to the normal distance from the wall surface is set to zero.

In the present case, the inlet boundary corresponds to the upstream boundary of the 11 Zonal-grids representing the stator. Characteristic boundary condition is used to specify the subsonic flow condition at the inlet. This approach needs four quantities to be specified. The four parameters chosen for the present study are as follows;

$$R_1 = w + \frac{2c}{\gamma - 1} \qquad (1)$$

$$R_3 = \frac{p}{\rho^{\gamma}} \qquad (2)$$

also, inlet flow angle, which leads to the following equation;

$$v_{inlet} = 0 \quad \text{and} \quad u_{inlet} = 0 \qquad (3)$$

In the above equations, p, ρ and c represent pressure, density and sonic velocity, respectively. The velocities in the x, y and z directions are represented by u, v and w, respectively. A Reimann invariant which is chosen as the fifth parameters, which are required to update the points on this boundary, is written below

$$R_2 = w - \frac{2c}{\gamma - 1} \qquad (4)$$

This value is obtained by extrapolation from the interior points.

The extreme left and extreme right boundary of the 11 zonal grids for stator are treated by simple periodicity boundary conditions. The outlet of 11 stator airfoils and inlet of 14 rotor airfoils is the interface of the stator and rotor, where one zone is moving relative to the other. In this zonal interface an implicit flux conservation technique is used to pass the information between the two zones. The exit corresponds to the downstream boundary of the rest 14 zonal grids representing rotor. For an axially subsonic outflow, the first four characteristics

are outgoing and are obtained by implicit extrapolation, so only the fifth characteristic variable need to be set. The average change in the characteristic is determined to achieve the specified average exit pressure at the mid-span from the local equilibrium conditions. A partially non-reflective procedure developed by Erdos(1977) is used.

In fact the flow developing on a turbomachinery blade starts as laminar, but in most situations it inevitably becomes turbulent. Transition from laminar to turbulent in the boundary layer, which often causes a significant change in operational performance of the machinery, is generally influenced by the free-stream turbulence activity, existence of laminar separation bubble and also by the pressure gradients. Also, the flows in turbomachinery blade passages are often highly rotational and dominated by viscous effects. In the case of stator rotor interaction, the wakes leaving the stator blade passages periodically impinging to the rotor blades. This fact results in considerable vortex stretching and change in turbulence activity in the rotor blade passage. Rai(1987a) in his work used an empirical turbulent model which is developed to predict boundary layer behavior in stationary cascades. That is why in his three-dimensional calculations the agreement between the experiment and prediction is good for stator, but not that good in the case of rotor. In the present study in order to capture the vortex stretching effect and the change in turbulence activity due to periodic interaction of wakes with rotor blade, an improved low Reynolds number version of turbulent model by including the secondary straining effect of swirl is used. To capture the near wall viscous effects proper grid resolution is used. At the wall y+ is kept less than 1.

RESULTS AND DISCUSSIONS

In this section are presented the results obtained for the stator-rotor configuration shown in Fig.1. By performing about three iterations at each time step, the equations of motion along with the boundary conditions discussed above are solved to obtain our results. In order to eliminate the initial transients and establish a solution that is periodic in time, nearly seven cycles ate required. A cycle represents the rotor motion through an angle equal to 2π /N. N is defined as the number of stator airfoils. All these facts mentioned above are similar to those observed by Rai(1987b). In the present study constant time step value is used to perform the computation.

Inlet pressure p_∞ and density ρ_∞ are used to non-dimensionalize the dependent variables and followings are obtained;

$w_\infty = M_\infty \sqrt{\gamma}$

$u_\infty = 0 \quad v_\infty = 0$ This corresponds to axial inlet flow.

Where, M_∞ means the inlet Mach number. In the present computations inlet Mach number of 0.07 was used. Based on the dependent variables mentioned above, the Riemann invariants that are prescribed at the inlet are determined. The desired flow coefficient u/w (0.78 in this case) and the axial velocity (w) are used to determine the rotor velocity. Since, the Riemann invariants and not the dependent variables themselves are prescribed as the boundary conditions at the inlet, when the solution becomes periodic in time, the values of u, v, w, p and ρ obtained at the inlet are different from those used to determine Riemann invariants. In the present study to obtain the flow coefficient, which corresponds to right value of rotor velocity, results based on preliminary 2-dimensional computation are used. Therefore in the present study no iterative process is carried out.

The Reynolds number corresponds to the experimental flow Reynolds number is used in the present computation. As it is discussed above an improved two-equation low-Reynolds number k-τ turbulence model is used to determine the eddy viscosity in the present computation. The detail of the modeling is available in the work of Biswas(2002). A brief outline of the modeling will be given below.

Modeling of Limiting Behavior of Wall Turbulence and secondary straining effect of swirl

In order to incorporate the near-wall effects into the standard k-ε model, some low-Reynolds-number damping factors are introduced. The purpose of these functions in different models is to provide a somewhat similar kind of modifying influence on the standard k-ε model. The application of different k-ε models by Biswas(1994) to predicting a flat plate transitional boundary layer led to the understanding that the existing k-ε models have some deficiencies in terms of modeling the low-Reynolds number damping functions. Some of the models assumed that the approximations that have been devised to handle near-wall low-Reynolds-number flows are equally valid for low Reynolds-number transitional flows. This is because these models could produce the correct blending between the (essentially laminar) viscous sub-layer and fully turbulent outer boundary layer region as shown by Nagano(1990), but failed to provide the correct stream-wise blending between the pre-transitional pseudo-laminar boundary layer and the post-transitional fully turbulent boundary layer flow. This study indicated that the models in which the low-Reynolds-number damping factors are defined as an explicit y dependence are less likely to predict accurate transition process, a fact that was also observed by Fujisawa(1990). Physically, anywhere near correct predictions of transitional boundary layer can be achieved by defining the low-Reynolds-number damping factors as a function of some quantity (for example turbulence Reynolds number R_{et}). This Ret is only a rather general indicator of the degree of turbulence activity at any x or y location in the flow rather than a specific function of location itself. Based on the understanding of characteristics of different low-Reynolds-number functions, the author in his previous work proposed a model in which these functions satisfy both the wall-limiting effect and the asymptotic behavior in the region away from the wall. In the case of gas turbine flow, where one set of blade row is rotating with respect to a static set of blade row, it is very important to consider the effect of swirl in the modeling of turbulence phenomena. Characteristics of local turbulence in the present work is accomplished by a k-τ turbulent model which is improved to take into account the effect of rotating turbulent flows. Since it is well known that the two-equation type turbulence model in its standard form is not adequate for taking into account the secondary straining effect of swirl. It is already reported in the open literature, that the secondary straining increases or decreases the turbulent length scale in the flow field depending on the stability of the straining field. In the standard two-equation model, the eddy viscosity is defined as a function turbulent kinetic energy and its dissipation rate and the model constant C_μ has a constant value of 0.09. In the present model eddy viscosity is modeled as a Richardson number-dependent modified eddy viscosity. Based on this approach, an improved low-Reynolds-number k-τ model for rotating flows is developed by formally operating on the algebraic Reynolds stress model to modify eddy viscosity.

Multi-Stator and rotor calculation

As it is mentioned before that the present computation is carried out using 11 stator and 14 rotor airfoils. As compared to Rai's previous work (1987a),(1987b), the resulting ratio of rotor to stator is exactly the same as that of experimental ratio (28/22). Consequently the problem of re-scaling is avoided in our study. In addition it can be shown that only the higher harmonics result in propagating pressure signals. The lower harmonics result in decaying pressure signals. Since the higher harmonics are much smaller in magnitude than the lower harmonics, the pressure signals reaching the exit boundary can

also be expected to be much smaller in magnitude. Hence the reflective properties of the exit boundary conditions play a smaller role in determining the unsteady pressure on the airfoils.

Measured values of Dring(1982) on time-averaged pressures and pressures amplitudes at mid-span for an axial gap of 15% are used to assess the present method. In Fig.3 and 4 are plotted the variation of computed and measured variation of time averaged pressure coefficient (C_p) along the axial distance of the stator and rotor airfoils in the mid-span region, respectively.

The following definition is used for pressure coefficient;

$$C_p = \frac{p_{avg} - (p_t)_{inlet}}{1/2\rho_{inlet} w_{inlet}^2}$$

Where, the static pressure averaged over one cycle is p_{avg}, $(p_t)_{inlet}$ represents the average total pressure at the inlet of the mid-span. At the inlet of the mid-span, average density and the velocity of the rotor are represented by ρ_{inlet} and w_{inlet}, respectively. Clearly, the computed and measured data showed a good agreement. Also, results are of better quality than that obtained by Rai in his one stator-one rotor and three stator-four rotor calculations. At the trailing edge of the pressure side of the stator, a small separation bubble was observed. This is seen as a spatial fluctuation in pressure toward the trailing edge of the stator. In both the measured and computed results (Fig.4), there occurs a small separation bubble near the trailing edge circle of the rotor. This bubble is considered as a sharp dip and rise of C_p toward the trailing edge on the pressure side.

The amplitude of temporal pressure fluctuation is a indicator of the unsteadiness of the flow. In Fig.5 and 6 are plotted the variation of pressure amplitude along the axial distance of the rotor and stator in the mid-span region. The amplitude of temporal pressure fluctuation is represented as follows;

$$C_p = \frac{p_{\max} - p_{\min}}{\frac{1}{2}\rho w^2}$$

Where, the maximum and minimum pressures that occur over a given cycle at a given point are p_{max} and p_{min}, respectively. Clearly there is a marked improvement over the numerical results presented by Rai, using one-stator and one-rotor and three-stator and four-rotor in his computations. The numerical amplitude distribution shows that most of important features that are found in the experimental results. The predicted distribution of pressure amplitude exactly matches the experimental data. Also, the positions of experimental and numerical peaks are in very good agreement. The numerical data show an amplitude minimum on the suction side of the stator, as do the experimental data. The experimental configuration of 22 stator and 28 rotor resulted in only the higher harmonics in time giving rise to propagating waves; the lower harmonics gave rise to decaying signals. Since the higher harmonics are much smaller in magnitude, the unsteady pressures that reach the exit boundary are much smaller in the case of the experiment. Most of the difference between theory and experiment observed in the case of Rai's results due to low rotor-stator ratio and the effect of re-scaling is solved in the present case. The results also indicated that temporal behavior in the case of rotating machinery depends strongly on the rotor-stator ratio.

The present 3-d calculation leads us to have a good understanding of the hub to tip distribution of the time averaged pressure coefficient also. Here, the assessment of the results of computation with the measured data on time averaged stator and rotor surface pressure coefficient obtained with an axial gap of 50% (the numerical data were obtained with an axial gap of 15%) are presented. However, Dring(1982) in his work indicated that the axial gap has only a negligible effect on time averaged surface pressure on stator and rotor. Hence, the performance of the present numerical approach can be tested to a large extent comparing computed and measured data for the 50% axial gap. In Figures 7a - 7g are plotted the measured and computed time averaged pressure coefficients, C_p, distribution on the stator at 2.0%, 12.5%, 25.0%, 50.0%, 75.0%, 87.5%, and 98.0% of the span, respectively. The line and the symbol represent the computed and measured data, respectively. The pressure-side static pressure distribution is almost the same as that at mid-span is a common feature to all the figures (7a-7g). There occur considerable changes in the suction side pressures between the hub and the tip. The pressure distribution near the hub (Fig.7a-b) indicated a similar type of flow behavior, that is, the airfoil is unloaded in the forward portion, and loaded in the rear portion relative to mid-span values. As compared to the case near the hub, pressure distribution at 25% span is closer to that in the mid-span, that is, there occur less loading and unloading in the rear and forward portion. From the results presented in Fig.7c-7g it is observed that this trend of increasing and decreasing load on the forward and rear portion continued all the way to the tip. The secondary flows corresponding to the horseshoe vortices at the hub and tip, the twist on the stator and the increasing stator passage width with increasing radius is expected to results in this changing load on the suction side. The computes and measured data compare very well all the way from the hub to the tip.

In Fig.8a- 8f are plotted the time averaged surface pressure coefficient (C_p) distribution on the rotor at 2.0%, 12.5%, 25.0%, 50.0%, 75.0%, and 87.5% of the span, respectively. Here also, the line and the symbol represent the computed and measured data, respectively. As it is mentioned above, in the case of stator-rotor interaction, the wake leaving the stator blade passages, periodically impinging to the rotor blades. This fact results in considerable vortex stretching and change in turbulence activity in the rotor blade passages. Therefore the boundary layer growth in the rotor blade passages strongly influenced by the transport of turbulence by the wake from the stator and there occur periodic transition from laminar to turbulent flow. The passage vortex impinging almost normally on the rotor surface resulted in higher pressure in the mid-chord region on the suction side, as can be observed from the results presented in Fig.8. The experimentally observed flow phenomena in the rotor blade passages are predicted nearly correctly by the present method as compared to those presented by Rai. Since, a turbulence model developed including straining effect is used in this study.

Figures 9a-9b show pressure contour at various time instants (time interval of $1.24X10^{-3}$ sec) in the mid-span region for the whole configuration formed by 22 stator and 28 rotor airfoils. These figures clearly show the main features of the time-averaged pressure distribution of figs.5 to figs.8. That is, the expansion and subsequent recompression of the flow on the suction side of the stator and rotor, and the almost constant pressure region followed by an expansion on the pressure side of the stator and rotor. Unlike the one-rotor/one-stator results of Rai(2) the pressures in the different rotor and stator channels are out of phase. This figure helped to have a good understanding of the flow behavior in this complex configuration. The suction side pressure minimum at this mid-span location occurs on the airfoil for both the stator and the rotor.

SUMMARY

Unsteady Navier-Stokes solver has been developed to study three-dimensional practical multi-stator and multi-rotor interaction problem. The solver used patched grids that move relative to each other to simulate the motion of the rotor airfoils with respect to the stator airfoils. The integration method is a MUSCL-type TVD upwind scheme which is spatially third order accurate and temporally second order accurate. Upwind finite difference scheme is set in an iterative implicit framework. The solver is used to simulate subsonic flow past a turbine stage for which considerable data exist.

Numerical results were obtained for 11 stator and 14-rotor configuration to satisfy the experimental rotor to stator ratio. Results in the form of time averaged surface pressures, surface pressure amplitudes (corresponding to the pressure fluctuations in time), and instantaneous passage pressure contours are presented for the present configuration. A very good agreement between measured and computed time averaged surface pressure is obtained. The surface pressure amplitudes is also predicted very well. This fact indicates that the surface pressure amplitudes (that is the unsteady flow due to the relative movement of the rotor with respect to the stator) strongly affected by the ratio of rotor to stator.

REFFERENCES

Dring, R. P., Joslyn, H. D., Hardin, L. W., and Wagner, J. H., 1982, "Turbine Rotor-Stator Interaction," ASME Journal of Engineering for Power, vol.104, pp.729-742.

Rai, M. M., 1987a, "Navier-Stokes Simulations of Rotor-Stator Interaction Using Patched and Overlaid Grids," AIAA Journal of Propulsion and Power, vol.3, No.5, pp.387-396.

Rai, M. M., 1987b, "Unsteady Three-Dimensional Navier-Stokes Simulation of Turbine Rotor-Stator Interaction," Presented at the AIAA/SAE/ASME/ASEE 23rd Joint Propulsion Conference, San Diego, CA, June29-July2, AIAA Paper No. 87-2058.

Rai, M. M., and Madavan, N. K., 1990, "Multi-Airfoil Navier-Stokes Simulations of Turbine Rotor-Stator Interaction," ASME Journal of Turbomachinery, vol.112, pp.377-384.

Biswas, D., et. al.,2002, "Application of a Two-equation Low-Reynolds Number Version Turbulent Model to Transitional Boundary Flows," 32 AIAA Fluid Dynamics Conference, St. Louis, US, AIAA Paper No.2002-2748.

Erdos, J. I., Alzner, E., and McNally, W., 1977, "Numerical Solution of Periodic Transonic Flow Through a Fan Stage," AIAA Journal, Vol.15, No.11, pp.1559-1568.

Biswas, D., et. al.,1994, "Calculation of Transitional Boundary Layers with an Improved Low-Reynolds Number Version k-ε Turbulence model," ASME Journal of Turbomachinery, vol.116, pp.765-773.

Nagano, Y., and Tagawa, M., 1990, "An Improved K-ε Model for Boundary Layer Flows," ASME Journal of Fluid Engineering, Vol.112, pp.33-39.

Fujisawa, N., 1990, "Calculations of Transitional Boundary Layer with a Refined Low-Reynolds-Number Version of a K-ε Model of Turbulence," Engineering Turbulence Modeling and Experiments, Elsevier Science Publishing Co.,pp.23-32.

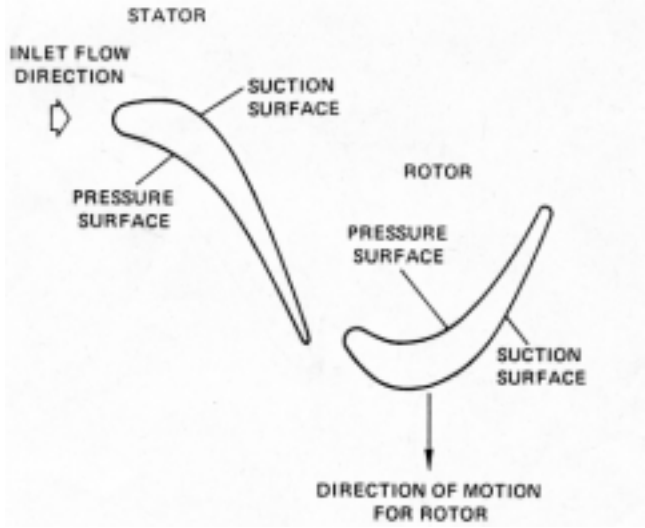

Fig.1 Rotor-stator configuration of Dring

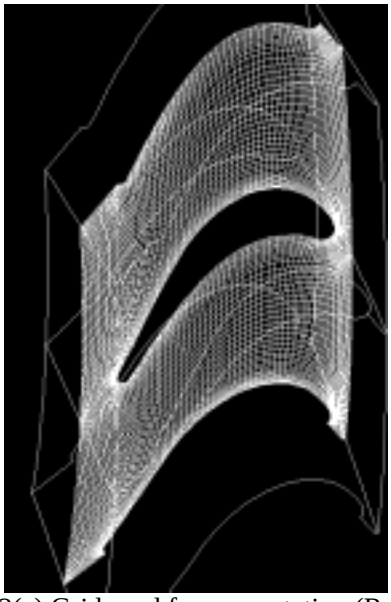

Fig.2(a) Grid used for computation (Rotor)

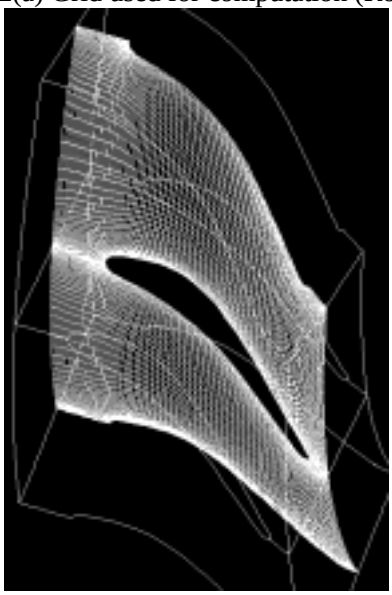

Fig.2(b) Grid used for computation (Stator)

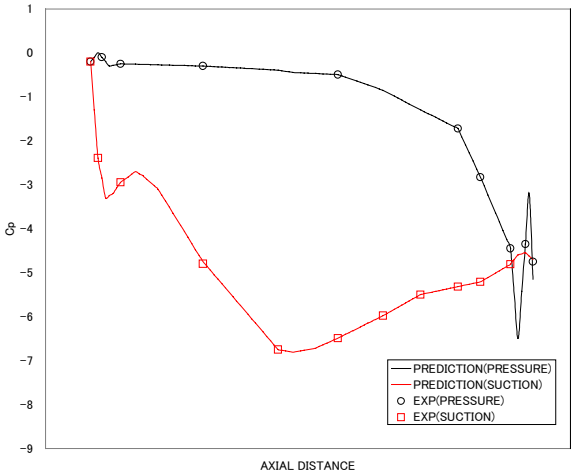

Fig.3 Time averaged pressure (Stator)

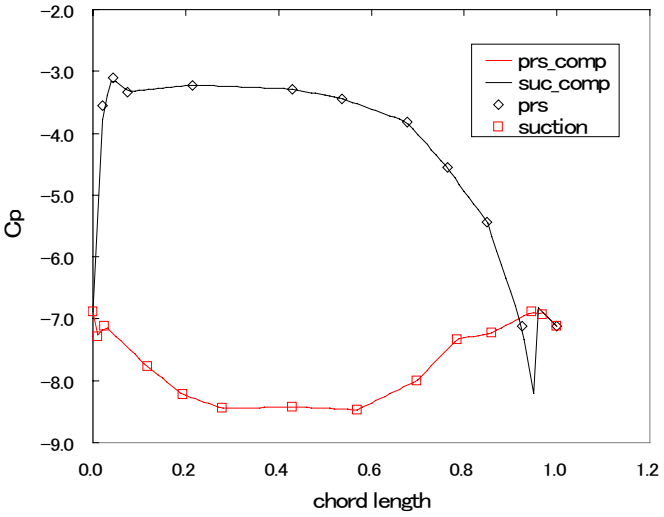

Fig.4 Time averaged pressure (Rotor)

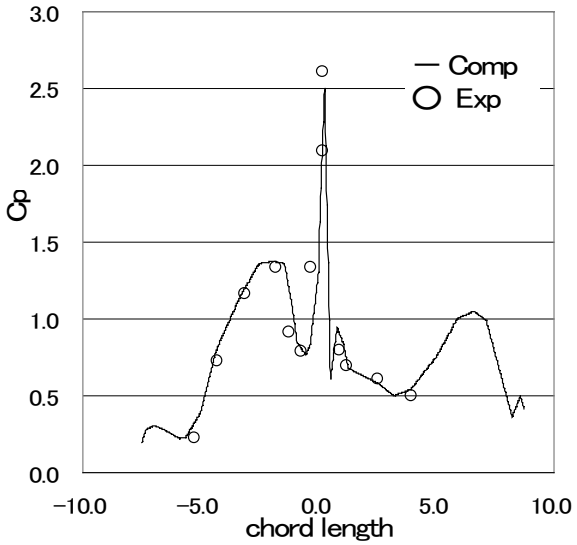

Fig.5 Pressure amplitude distribution on rotor

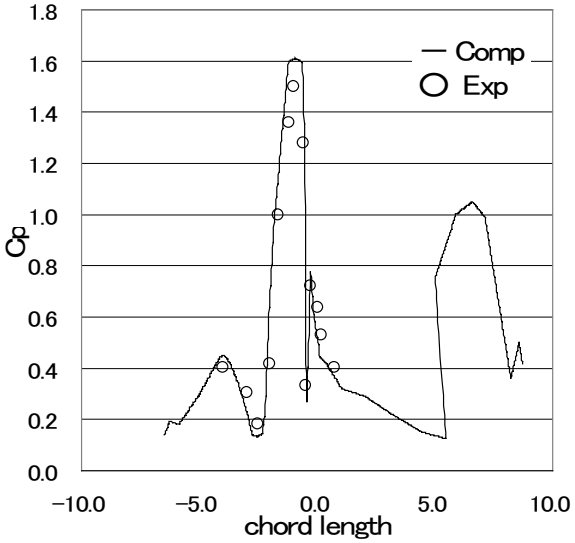

Fig.6 Pressure amplitude distribution on stator

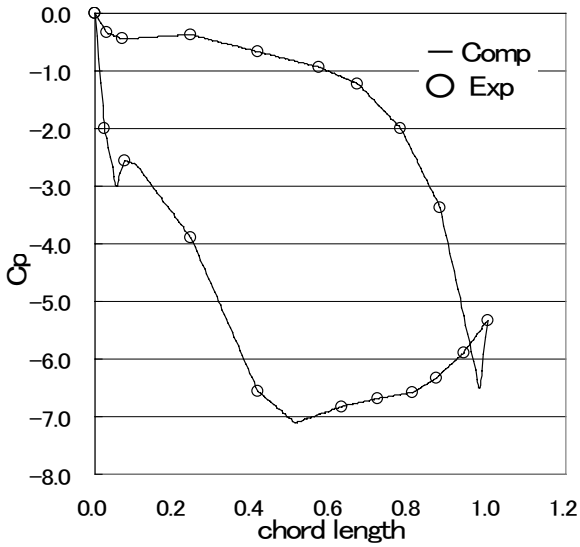

(a)

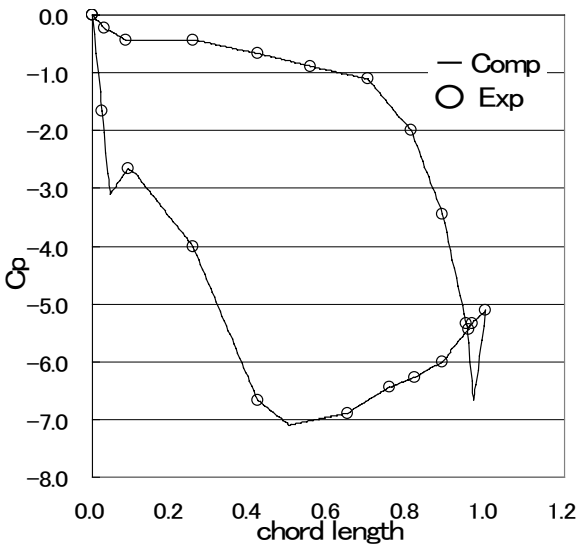

(b)

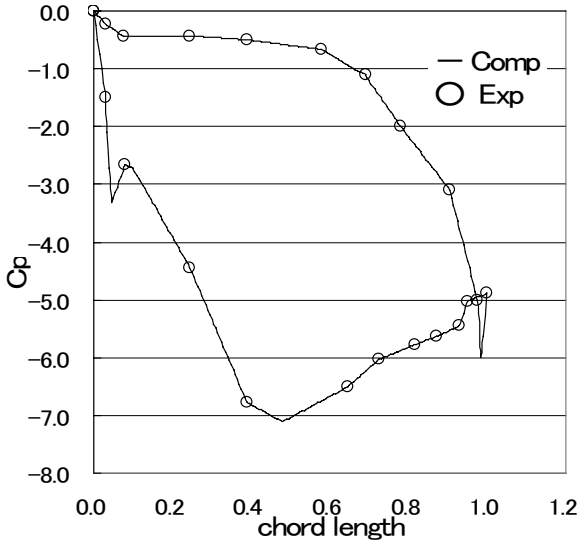

(c)

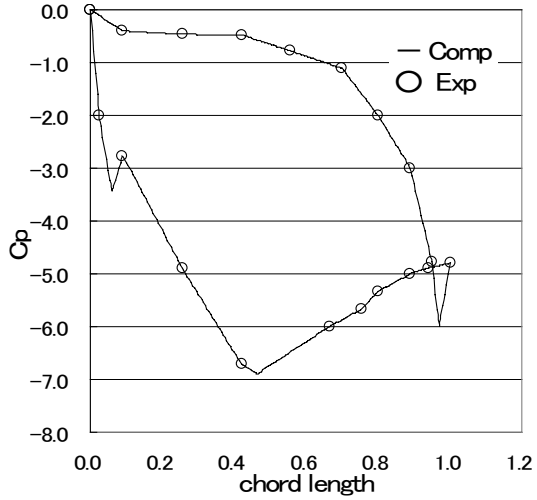

(d)

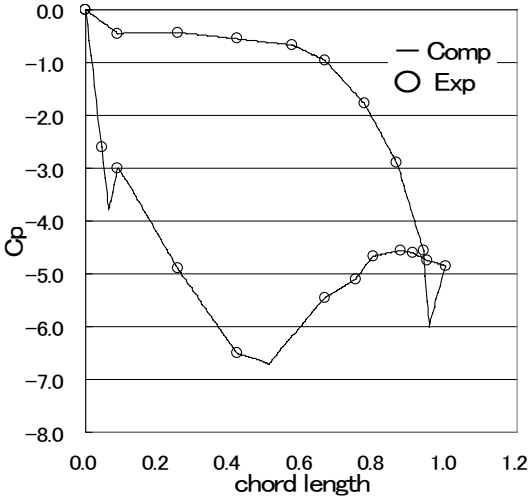

(e)

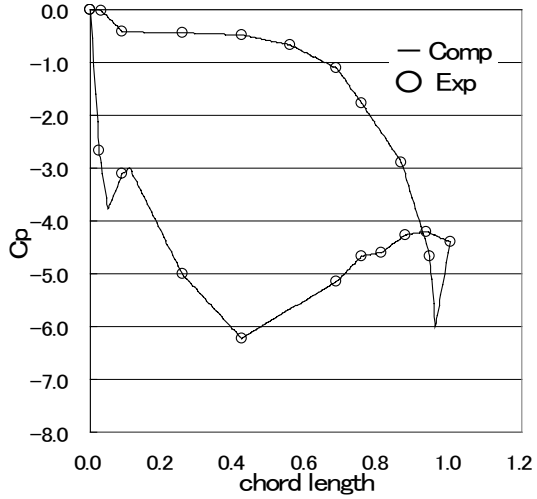

(f)

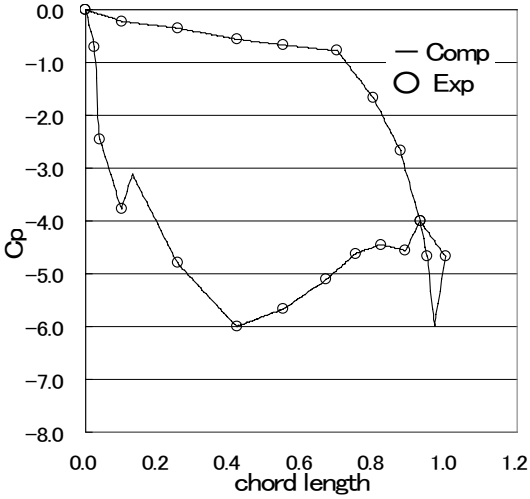

(g)

Fig.7Span variation of time averaged pressure distribution on the stator
(a) 2%, (b) 12.5%, (c) 25%, (d) 50%, (e) 75%, (f) 87.5% and (g) 98%.

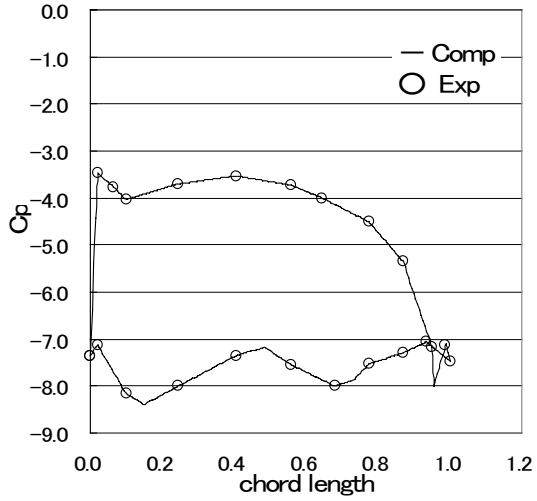

(a)

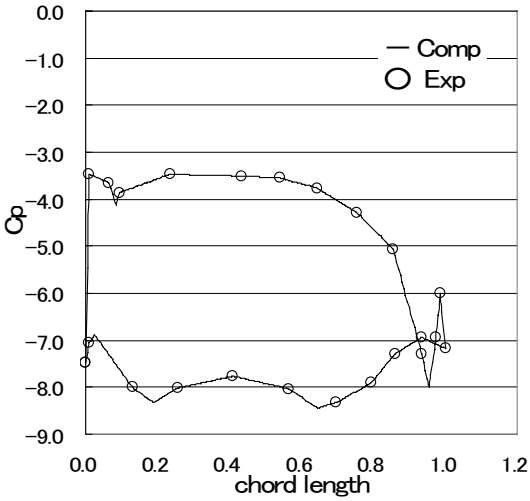

(b)

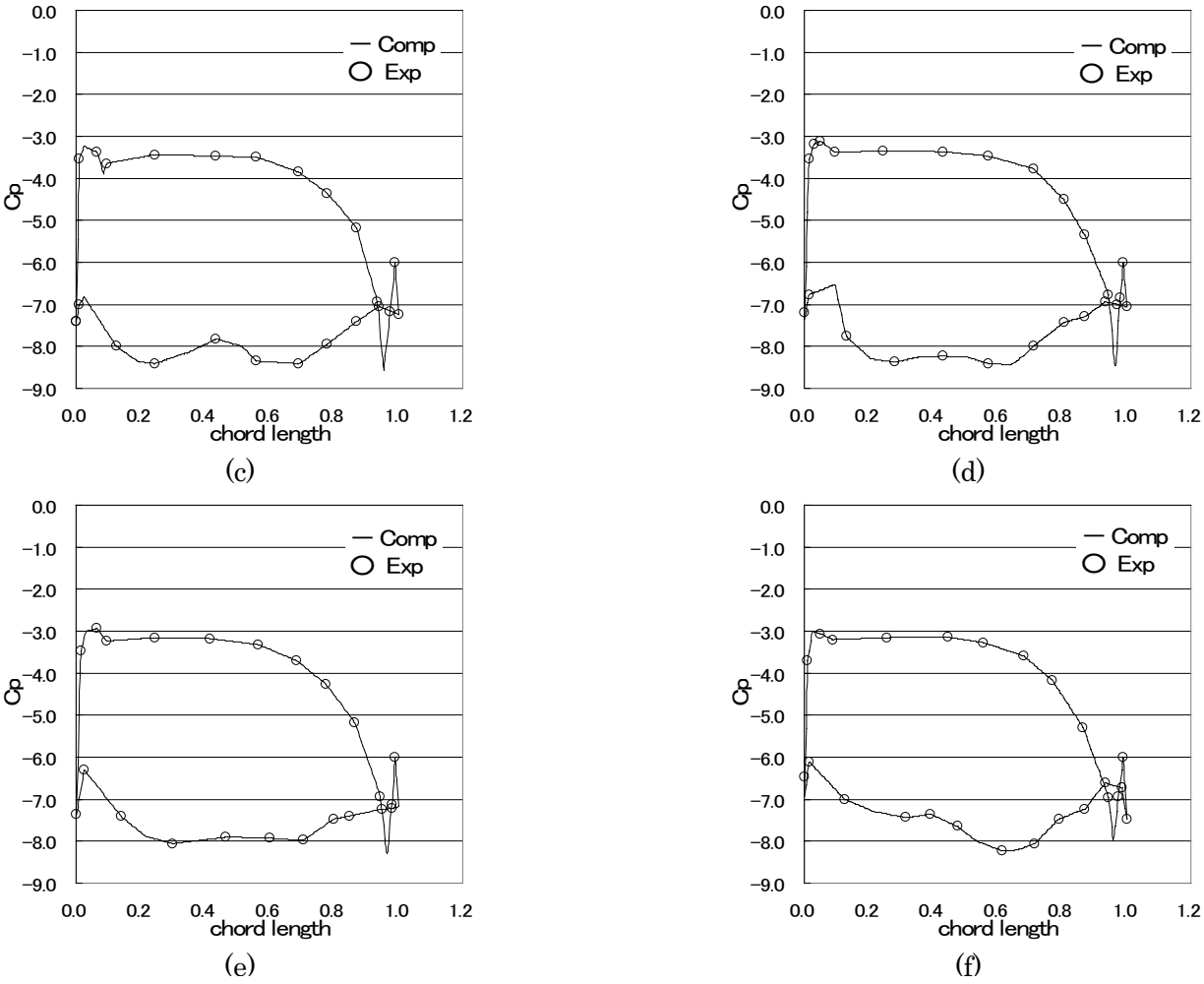

(c) (d)

(e) (f)

Fig.8 Span variation of time averaged pressure distribution on the rotor
(a) 2%, (b) 12.5%, (c) 25%, (d) 50%, (e) 75%, and (f) 87.5%

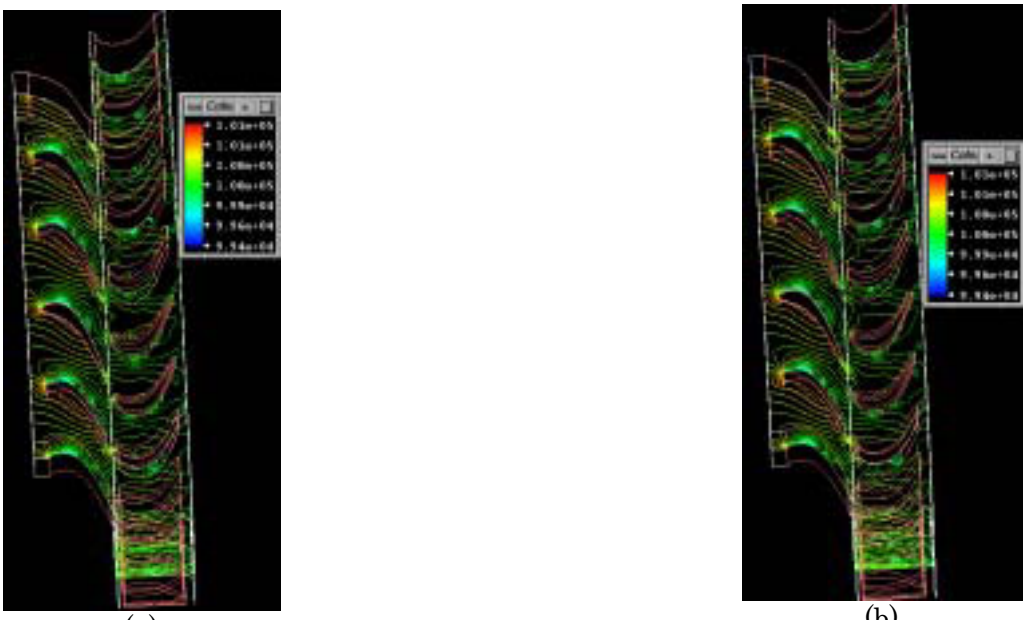

(a) (b)

Fig.9 pressure contour with time